ACS APPLIED ENERGY MATERIALS
Cite This: ACS Appl. Energy Mater. 2019, 2, 2305−2312
Article
www.acsaem.org

Pulsed Laser Deposition of $CsPbBr_3$ Films for Application in Perovskite Solar Cells

Hong Wang,[†] Yu Wu,[†] Meiyang Ma,[†] Shuai Dong,[†] Qi Li,[†] Jun Du,[‡,§] Hao Zhang,*[,†] and Qingyu Xu*[,†,‡]

[†]School of Physics, Southeast University, Nanjing 211189, China
[‡]National Laboratory of Solid State Microstructures, Nanjing University, Nanjing 210093, China
[§]School of Physics, Nanjing University, Nanjing 210093, China

Supporting Information

ABSTRACT: Organic−inorganic hybrid halide perovskite materials have attracted enormous interest in recent years due to their excellent photovoltaic properties, which are strongly limited by their instability. Solar cells based on the inorganic perovskite materials have been developed rapidly and exhibit excellent stability. The crystalline quality and composition of the perovskite layer play the key role in the efficiency of solar cells. Among the various film deposition techniques, pulsed laser deposition has the distinctive advantages of preparation of thin films of high crystalline quality and close duplication of the composition of the targets. In the work, we applied pulsed laser deposition to prepare a $CsPbBr_3$ thin film that displays good stability in a high-humidity environment. Single crystalline $CsPbBr_3$ powders were grown first by a solution method to prepare the target. The $CsPbBr_3$ plasma produced by focused pulsed laser can permeate into the mesoporous TiO_2 layer and distribute uniformly inside. The thickness of mesoporous TiO_2 and $CsPbBr_3$ layers has a critical influence on device performance. The device with optimization of the layer thickness can achieve the highest power conversion efficiency of 6.3%.

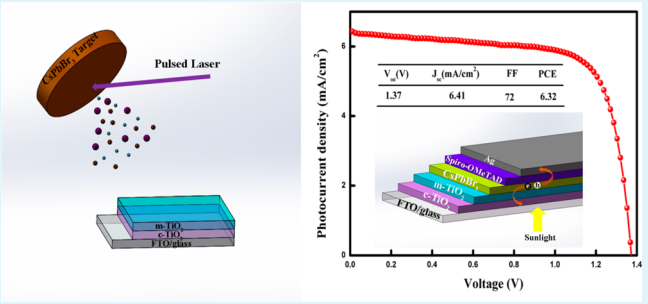

KEYWORDS: *inorganic perovskite, pulsed laser deposition, $CsPbBr_3$ film, stability, solar cells*

1. INTRODUCTION

Solar energy has attracted a lot of interest and has developed very fast as a clean renewable energy, due to the serious global environment crisis.[1−3] Organic−inorganic perovskite materials possess outstanding photophysical and electronic properties, such as high power conversion efficiency (PCE), long charge diffusion length, appropriate direct band gap, low-density traps, and low cost, etc.[2,4−6] Hence, organic−inorganic perovskite solar cells (PSCs) develop rapidly with their PCE increasing up to 23.2% within several years.[7−11] ABX_3 (A = $CH_3NH_3^+$ (methylammomium, MA^+), $CH(NH_2)_2^+$ (formamidinium, FA^+), or Cs^+; B = Pb^{2+}, Sn^{2+}; X = I^-, Br^-, CI^-) is the most common formula for the perovskite materials.[12−15] Unfortunately, organic−inorganic perovskite absorbers are susceptible to moisture corrosion and photo-oxidation that cause instability and decomposition because of the organic cations.[16−18] Upon substitution of Cs^+ for the organic cation, cesium-based inorganic halide perovskite materials ($CsPbX_3$ (X = halide)) are good candidates which show a similar crystalline structure and photoelectric properties.[10,19] Recently, the solar cells based on the inorganic lead halide perovskite have developed very quickly, due to their high stability under illumination and at an elevated temperature.[11,19]

Spin-coating is the most common method for the preparation of PSCs. However, spin-coating is difficult to use for deposition of films of high crystalline quality and fabrication of large-area PSCs for commercialization.[9,16] Therefore, we introduce pulsed laser deposition (PLD) to the preparation of PSCs, which has been widely used in the deposition of various materials to thin films.[20,21] There are many advantages of PLD, such as abundant sorts of target materials, low cost, convenient operation, controllable deposition conditions, and so on.[22] In addition, high-quality films can be easily fabricated using PLD by controlling the substrate temperature, vacuum pressure, laser parameters, and so on.

In this paper, we apply PLD to prepare $CsPbBr_3$ thin films, instead of the conventional solution technique. PLD technology is a mature technology that can deposit various films on a large area with high uniformity and flatness, which is very challenging for the conventional solution method. Laser bombardment of the $CsPbBr_3$ target to form a densely stacked $CsPbBr_3$ film is of great significance for high-performance

Received: January 20, 2019
Accepted: March 4, 2019
Published: March 4, 2019

DOI: 10.1021/acsaem.9b00130
ACS Appl. Energy Mater. 2019, 2, 2305−2312

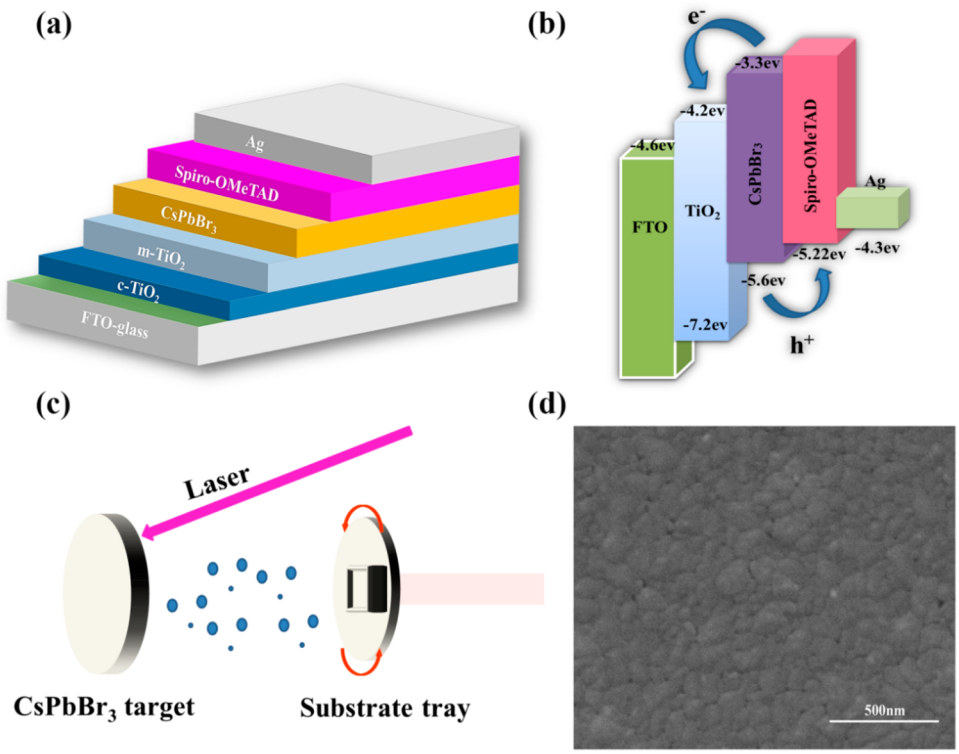

Figure 1. (a) Schematic diagram of perovskite solar cells. (b) Energy-level diagram of $CsPbBr_3$-based PSCs and charge transportation processes. (c) Schematic diagram of $CsPbBr_3$ thin films prepared by PLD. (d) The plane-view SEM image of $CsPbBr_3$ film.

PSCs with high stability. The $CsPbBr_3$ film prepared by PLD is thin and dense with good stability in a high-humidity environment. It is confirmed that $CsPbBr_3$ can permeate into the whole mesoporous TiO_2 (m-TiO_2) layer. By optimizing the thickness of m-TiO_2 and $CsPbBr_3$ layers, the short-circuit current density (J_{sc}) of 6.4 mA cm^{-2}, open-circuit voltage (V_{oc}) of 1.37 V, fill factor (FF) of 72%, and PCE of 6.3% have been achieved.

2. EXPERIMENTAL SECTION

2.1. Methods. The $CsPbBr_3$ target was prepared from $CsPbBr_3$ single crystal powders, which were grown by an inverse temperature crystallization (ITC) method.[23] CsBr and $PbBr_2$ (1:2 molar ratio) were dissolved in dimethyl sulfoxide (DMSO) by heating in a sand bath from room temperature to 70 °C. Then, 13.6 g of cyclohexanol (CyOH) and 24.2 g of dimethylformamide (DMF) were mixed and added into the solution quickly. The solution was heated slowly to 110 °C at the heating rate of 1 °C/min. After 12 h, $CsPbBr_3$ single crystal powders were precipitated from the solution, which were cleaned by the 100 °C DMF and dried in the vacuum oven at 50 °C. Then, the crystals were ground and pressed to be the target (see Supporting Information, Figure S1).

F-doped SnO_2 (FTO) glass chosen as transport conducting substrates was cut and cleaned with detergent water, deionized water, and absolute ethyl alcohol by ultrasound successively. An 80 nm thick compact thin TiO_2 layer (c-TiO_2) was deposited on the clean substrate by spin-coating a tetrabutyl titanate solution (18% in absolute ethyl alcohol) at 5000 rpm for 30 s, followed by annealing at 500 °C for 40 min. Subsequently, a 200 nm thick m-TiO_2 layer was prepared by spin-coating the diluent with a weight ratio of m-TiO_2 paste/ethyl alcohol 1/8 at various speeds for 20 s and then annealed at 550 °C for 1 h.

Then, the substrate and target were put into the PLD chamber with base pressure of less than 10^{-3} Pa. The distance between target and substrate was 5 cm, and the substrate temperature was 320 °C. The $CsPbBr_3$ target was ablated by an excimer laser with wavelength of 248 nm, energy of 100 mJ, and frequency of 5 Hz. The thickness of films was controlled by the pulse number. After the deposition, the film was further annealed at 350 °C for 2 h in the chamber.

Finally, a 250 nm thick hole transport layer (HTL) was deposited by spin-coating the solution, which was mixed with 288 μL of TBP, 175 μL of Li-TFSI solution (520 mg of Li-TSFI in 1 mL of acetonitrile), 290 μL of Co-TFSI solution (300 mg of Co-TFSI in 1 mL of acetonitrile), and 20 mL of chlorobenzene together, on the $CsPbBr_3$ layer at 4000 rpm for 30 s. After one night in the glovebox, a 110 nm thick Ag layer was deposited on the HTL as back electrode by thermal evaporation at the rate of 0.2−0.3 Å s^{-1} in the chamber under the base pressure of 10^{-4} Pa.

2.2. Measurements. The crystalline structures were studied by X-ray diffraction (XRD, Rigaku Smartlab3) with Cu Kα radiation. A scanning electron microscope (SEM, FEI Inspect F50) was used to study the surface and cross-sectional morphologies of the films, and the elemental distribution was studied by the attached energy-dispersive X-ray dispersive spectroscope (EDX). The absorption spectra were obtained by an ultraviolet−visible spectrophotometer (HITACHI U-3900). Photoluminescence (PL) steady-state measurements were performed on a spectrofluorometer (Fluorolog3-TCSPC, Horiba Jobin Yvon). Time-resolved photoluminescence (TRPL) was recorded by an FLS920 spectrometer (Edinburgh Instruments). Atomic force microscopy (AFM) was performed on a BioScope Resolve. Current−voltage (I−V) curves were measured by the Keithley 2400 under a solar simulator (Newport oriel 91.192), which produced the illumination of (AM1.5, 1000 W m^{-2}) in air. Incident-photon-to-current conversion efficiencies (IPCE) were obtained by the IPCE measurement system from the Newport Co. The fluorescence of the $CsPbBr_3$ film was obtained under the ultraviolet source (ZF-1A) from Shanghai Qinke Analytical Instrument Co.

3. RESULTS AND DISCUSSION

Figure 1a shows the schematic structure of the solar cell device consisting of FTO/c-TiO_2/m-TiO_2/$CsPbBr_3$/Spiro-OMe-

DOI: 10.1021/acsaem.9b00130
ACS Appl. Energy Mater. 2019, 2, 2305−2312

TAD/Ag. Under sunlight illumination from the transparent FTO glass, photogenerated electrons and holes will be released by the $CsPbBr_3$ layer. Through the local electric field, electrons will be injected to the conduction band (CB) of TiO_2 (−4.2 eV) and then to FTO (−4.6 eV), and holes to the valence band (VB) of Spiro-OMeTAD (−5.22 eV) and then to Ag (−4.3 eV), as the schematic band diagram shows in Figure 1b. The $CsPbBr_3$ film prepared by the spin-coating method is not very uniform, and the effective utilization area is rather low. In order to solve such problems, PLD technology is introduced into the preparation of the $CsPbBr_3$ films. After the deposition of the m-TiO_2 layer, the $CsPbBr_3$ layer is deposited by PLD. Figure 1c displays the schematic diagram of the deposition process of PLD. After the ablation of the target, the sudden higher temperature makes the exposed area of the target surface form plasma, and ions sprout out toward the substrate. Due to the collisions among the ions and with TiO_2 particle surfaces, the projected ions can also penetrate into the sheltered spaces in the m-TiO_2 layer. The complete penetration of $CsPbBr_3$ in the m-TiO_2 layer with uniform distribution has been confirmed by the elemental mapping in Figure 2a,b, and the atomic concentration of Cs, Pb, and Br is

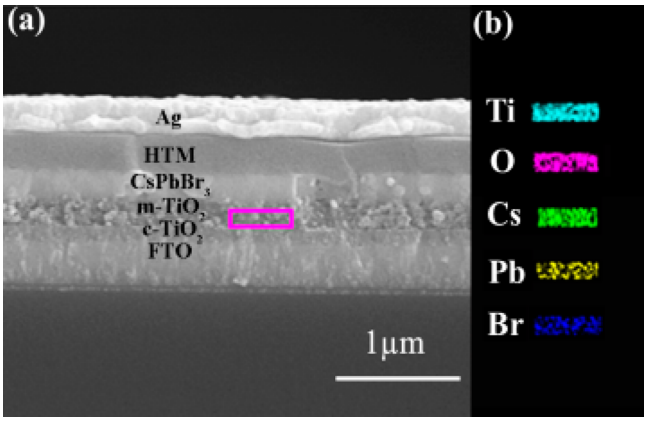

Figure 2. (a) Cross-sectional SEM image of $CsPbBr_3$-based perovskite solar cell. (b) Elemental distribution mapping images in the m-TiO_2 layer.

close to 1:1:3 (see Supporting Information Table S1 and Figure S2). After the filling of the space inside the m-TiO_2 layer, a continuous dense $CsPbBr_3$ layer is further formed, as the SEM image shows in Figure 1d.

In order to prove that the thin film prepared by PLD is compact and stable, we have grown $CsPbBr_3$ thin films on FTO substrates by spin-coating and PLD, respectively. It can be clearly seen from the photographs that the film prepared by PLD is denser and more uniform, as shown in Figure 3a. From SEM images top views, the $CsPbBr_3$ film prepared by PLD shows no obvious pores during the annealing process, which is flat and uniform, in comparison with the $CsPbBr_3$ film prepared by the spin-coating method (see Supporting Information, Figure S3). The organic solvent evaporates during the annealing process to cause voids.[24] In addition, the target used by PLD is only 2.5 cm in diameter and can be used many times to save materials. Therefore, PLD technology is superior to the traditional solution method. For organic perovskites, oxygen and moisture in air will have an effect on all $(CH_3NH_3)^+$ species on the surface that will be converted to water and volatile methylamine, which will not have a significant impact on Cs^+.[25] The 80 pulse $CsPbBr_3$ film prepared by PLD emits a distinct green light compared with the FTO glass by irradiation with a 365 nm wavelength ultraviolet source (Figure 3b). As shown in Figure 3c, we place the 80 pulse $CsPbBr_3$ film prepared by PLD in an environment with relative humidity of 80% and temperature of 27 °C to confirm the stability of the $CsPbBr_3$ film by observing the change of fluorescence with time. It can be seen that no significant decomposition of the $CsPbBr_3$ film was observed after 15 days of fluorescence intensity. For quantitative analysis, the fluorescence intensity of the 80 pulse $CsPbBr_3$ film with time is measured by PL in the same environment, and only a slight decrease is found due to the partial $CsPbBr_3$ film decomposition within 120 h (see Supporting Information Figure S4). Therefore, a thin and dense $CsPbBr_3$ film can be prepared by PLD, which is very stable in a highly humid environment.[26]

Figure 4a shows the XRD patterns of raw materials of CsBr and $PbBr_2$, and the precipitated $CsPbBr_3$ crystals. The XRD pattern of $CsPbBr_3$ crystals is significantly different from those of CsBr and $PbBr_2$, and all the diffraction peaks coincide well with standard data of the reported $CsPbBr_3$ crystal (ICSD card 97851).[23] The EDX data and EDX spectra of $CsPbBr_3$ powders are shown in Table S2 and Figure S5 in the Supporting Information. To check the crystalline structure, a single layer of the $CsPbBr_3$ film is directly deposited on the glass substrate, and the XRD pattern is shown in Figure 4b. As can be seen, all the diffraction peaks coincide well with those of $CsPbBr_3$ single crystal powders, and the variation of peak intensities is due to the preferred orientation of the lattice planes during the film growth. Both the light absorption spectrum and the steady-state PL spectrum of the $CsPbBr_3$ film (Figure 4c) reveal a peak at around 520 nm, which is close to the band gap of 2.38 eV.[9]

Figure 4d shows the TRPL spectrum of a complete device, which is fitted by a biexponential equation: $I(t) = I_0 + A_1\exp\left(-\frac{t-t_0}{\tau_1}\right) + A_2\exp\left(-\frac{t-t_0}{\tau_2}\right)$ (I_0 is a constant, A is the decay amplitude, and τ is the decay time.) The $CsPbBr_3$ film with a quenching layer of m-TiO_2 exhibits an average decay time of τ_{avg} = 4.8 ns that can be achieved with the equation $\tau_{avg} = \sum A_i\tau_i^2 / \sum A_i\tau_i$.[2,27] The detailed TRPL spectrum fitting results are shown in Table S3 (Supporting Information).

In perovskite solar cells, the full contact of the m-TiO_2 layer with perovskite materials ensures the maximum occurrence of photogenerated charge separation and charge injection.[27,28] Since the $CsPbBr_3$ film prepared by PLD penetrates in the m-TiO_2 layer, the effects of m-TiO_2 thickness and $CsPbBr_3$ thickness on device performance are investigated. Figure S6 (Supporting Information) shows that the root-mean-square (RMS) values of surface roughness of the m-TiO_2 layer are almost the same as that formed under various spin rotation speeds (1000, 2000, 3000, 4000, 5000 rpm), excluding the influence of the possible interface roughness of the m-TiO_2 layer on device performance. The thicknesses of m-TiO_2 layers are measured by SEM from the cross-sectional images to be 250 nm (1000 rpm), 200 nm (2000 rpm), 150 nm (3000 rpm), 120 nm (4000 rpm), and 100 nm (5000 rpm), respectively (see Supporting Information, Figure S7). We check the thickness dependence of PCE of the PSCs on the thickness of the m-TiO_2 layer by fixing the thickness of the

DOI: 10.1021/acsaem.9b00130
ACS Appl. Energy Mater. 2019, 2, 2305−2312

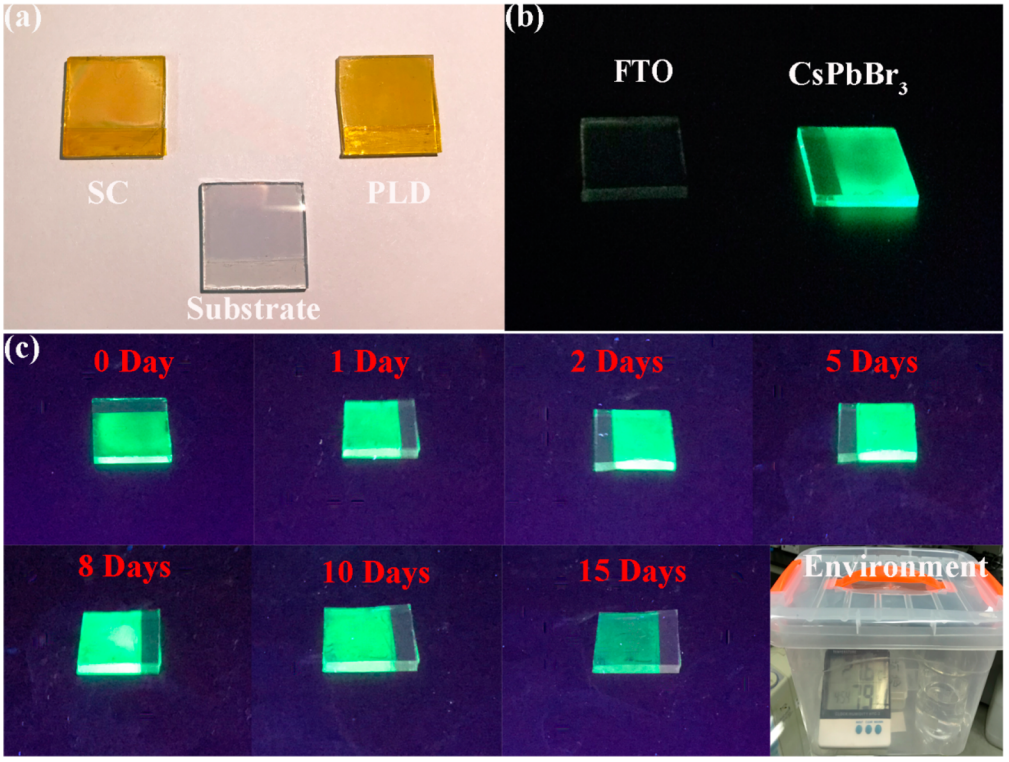

Figure 3. (a) $CsPbBr_3$ films are prepared on the same TiO_2 layer by spin-coating and PLD, respectively. (b) FTO glass and 80 pulse $CsPbBr_3$ film prepared by PLD are irradiated by the ultraviolet source. (c) The fluorescence of the 80 pulse $CsPbBr_3$ film prepared by PLD under ultraviolet illumination with time in ambient exposure (RH = 79%, T = 27.6 °C).

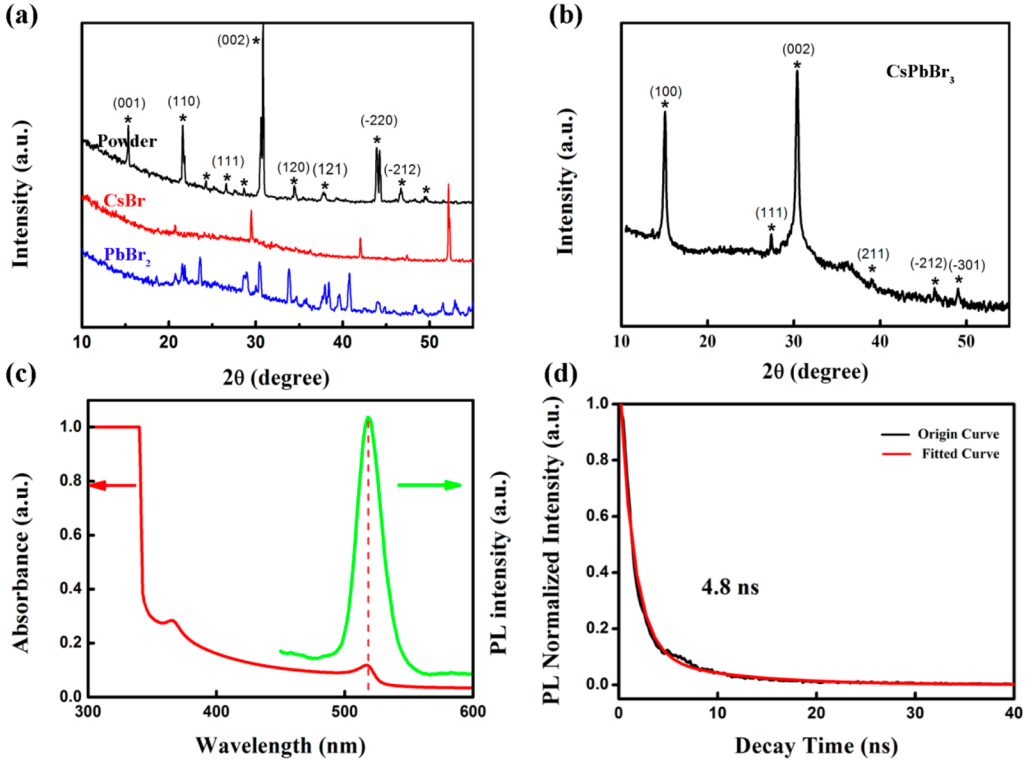

Figure 4. XRD patterns of (a) $CsPbBr_3$ powders, CsBr, $PbBr_2$, and (b) $CsPbBr_3$ thin film. (c) Light absorption spectrum and PL spectra and (d) transient-state PL spectrum of the $CsPbBr_3$ thin film.

$CsPbBr_3$ layer to 200 nm. As can be seen from Figure 5a, the PSCs with a thickness of the m-TiO_2 layer of 200 nm exhibit the best PCE. To understand the mechanism of the thickness dependence of the m-TiO_2 layer, we measure the resistance between two closed Ag electrodes by evaporating the Ag electrodes on the m-TiO_2 layer, and the resistances of various

DOI: 10.1021/acsaem.9b00130
ACS Appl. Energy Mater. 2019, 2, 2305−2312

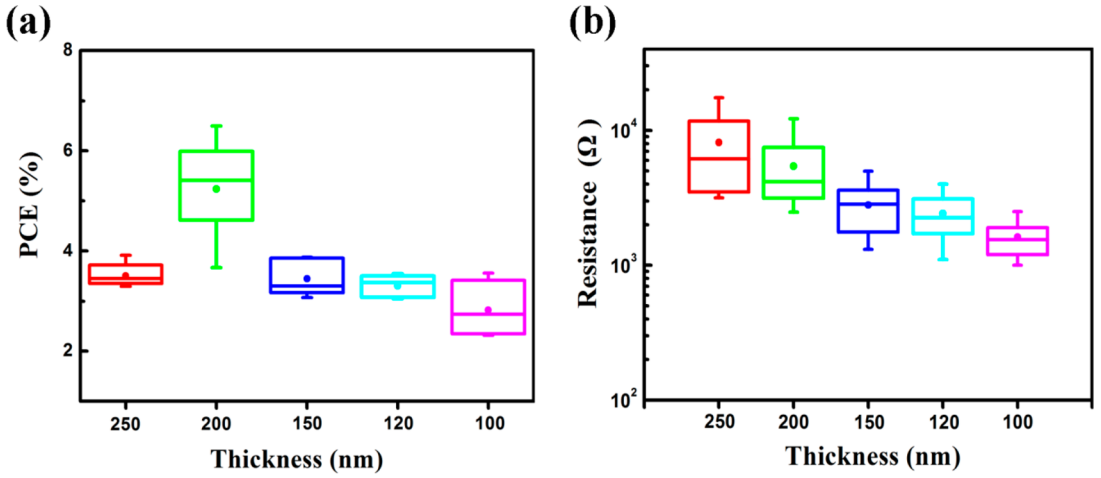

Figure 5. (a) PCE of the devices and (b) resistance values of the m-TiO_2 layer prepared by spin-coating with rotating speeds of 1000, 2000, 3000, 4000, and 5000 rpm.

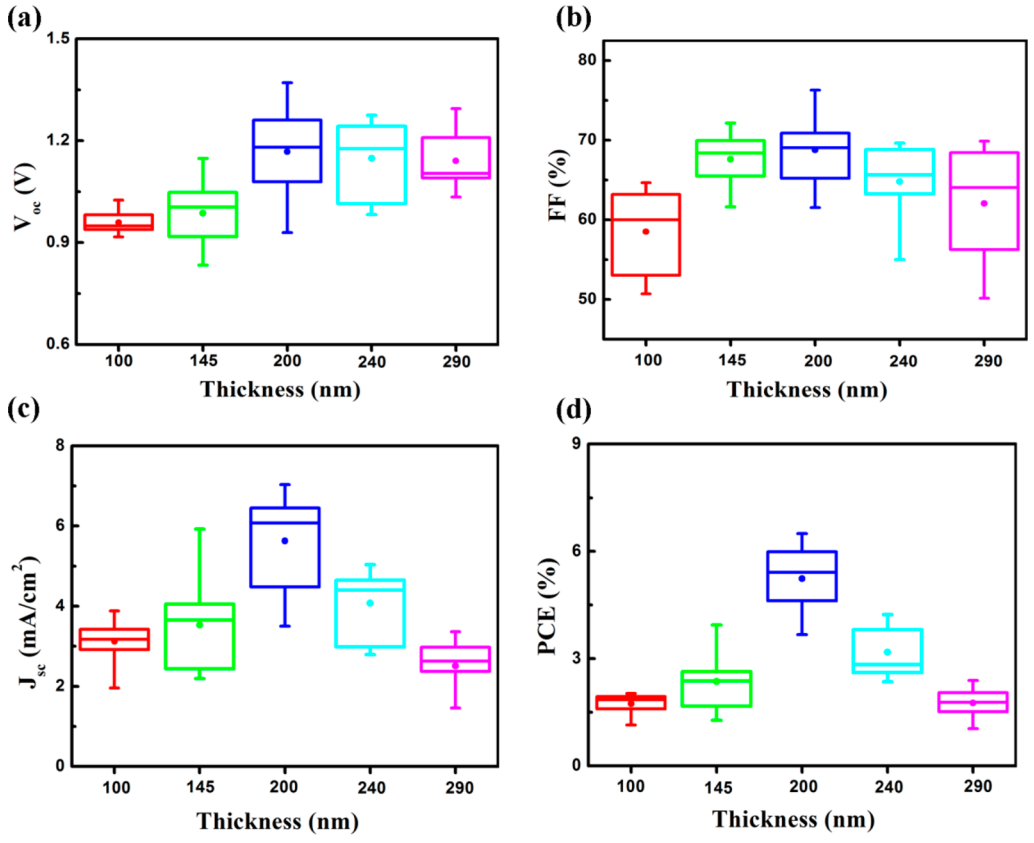

Figure 6. Range of (a) V_{oc}, (b) PCE, (c) FF, and (d) J_{sc} at the pulse number of 200, 300, 400, 500, and 600.

thicknesses are shown in Figure 5b. The resistance continuously decreases with an increase in the thickness of the m-TiO_2 layer. The PCE of the PSC with an m-TiO_2 layer of 250 nm is lower than that with the 200 nm layer, which is due to the larger resistance of the m-TiO_2 layer. The electrons injected into the conducting band of a thick m-TiO_2 layer are heavily compounded with the holes in perovskite. Although the resistance of the m-TiO_2 layer continuously decreases with an increase in the rotation speed, PCE continuously decreases with a decrease in the thickness of the m-TiO_2 layer below 200 nm, and a sudden drop of the PCE value can be observed with a decrease in the thickness of the m-TiO_2 layer from 200 to 150 nm. This is mainly due to the insufficient charge extraction capacity of the m-TiO_2 layer if it is not thick enough.[29] Moreover, an m-TiO_2 layer that is too thin cannot accept a perovskite thick enough to generate a narrow depletion region that cannot adequately separate electron−hole pairs.[30] In addition, the reduction of the m-TiO_2 layer thickness will lead to significant hysteresis and device instability which will affect device performance.[31] Therefore, the optimum thickness of m-TiO_2 layer is 200 nm for the following PSCs.

Next, we further study the influence of $CsPbBr_3$ film thickness prepared by PLD on PSCs device performance by fixing the thickness of m-TiO_2 layer to 200 nm. The thickness

DOI: 10.1021/acsaem.9b00130
ACS Appl. Energy Mater. 2019, 2, 2305−2312

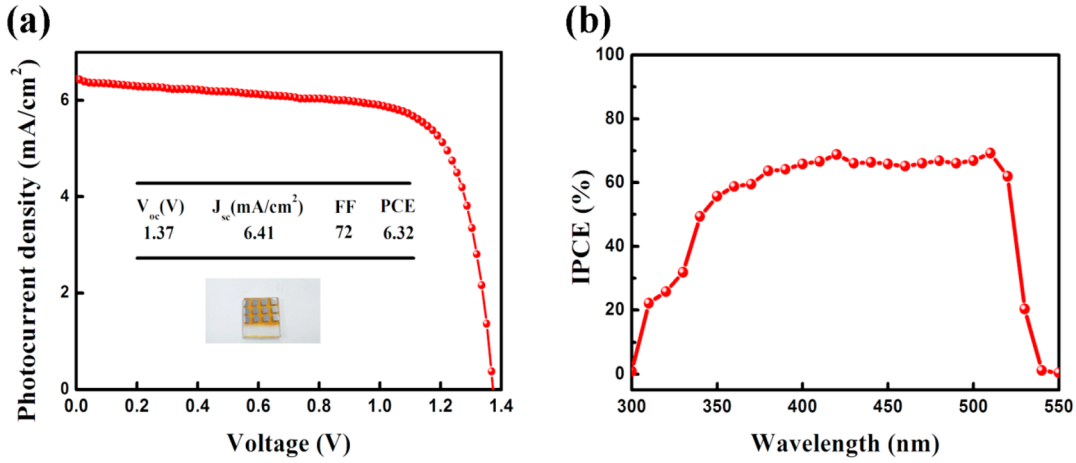

Figure 7. (a) $J-V$ curves and (b) IPCE spectrum of the $CsPbBr_3$-based solar cell with the best performance.

of the $CsPbBr_3$ film is determined by the number of laser pulses, as the thickness of the $CsPbBr_3$ layer is in linear dependence on the laser pulse number, which is shown in Figure S8 (see Supporting Information). The thicknesses of $CsPbBr_3$ films formed according to the different pulse number are 100 nm (200 pulses), 145 nm (300 pulses), 200 nm (400 pulses), 240 nm (500 pulses), and 290 nm (600 pulses), respectively. Compared with $MAPbI_3$-based PSCs, Figure 6a shows that the V_{oc} of $CsPbBr_3$-based PSCs is up to 1.37 V because of a wider band gap of $CsPbBr_3$ (2.38 eV). With an increase in the thickness of the $CsPbBr_3$ layer from 100 to 200 nm, V_{oc} gradually increases.[9,32] With a further increase of the thickness from 200 to 290 nm, the value of V_{oc} has not been significantly affected. Figure 6b shows that FF is also improved with an increasing thickness and then decreases when the $CsPbBr_3$ film thickness exceeds 200 nm. The average FF value of devices with a $CsPbBr_3$ layer 200 nm thick is the highest (about 68%). When the thickness increases from 200 to 290 nm, the average FF decreases by about 6%. It has been reported previously that low recombination resistance is present in the devices when the perovskite layer is too thin, which causes low FF and loss in the V_{oc}.[33] Furthermore, the main reason for an FF decrease is that the series resistances of cells increase with thickness. For thick $CsPbBr_3$ films, Spiro-OMeTAD hole transport materials are difficult to completely be in contact with the surface of $CsPbBr_3$ films, resulting in increased contact resistance between the $CsPbBr_3$ layer and HTL layer.[33,34]

Figure 6c shows that J_{sc} increases with an increase in the thickness up to 200 nm. As the thickness of the $CsPbBr_3$ film increases from 200 to 290 nm, the loss of J_{sc} is more significant than those of FF and V_{oc}. From Figure 6d, it is obvious that the efficiency of the device is significantly dependent on the thickness of the $CsPbBr_3$ layer. When the $CsPbBr_3$ layer is too thin or too thick, PCE drastically decreases to only around 1.5−2.5%. The devices with the $CsPbBr_3$ layer of 200 nm thickness have the best average PCE value of 5.3%, of which the highest PCE is 6.3%. With the thickness of the $CsPbBr_3$ layer being thinner than 200 nm, the light absorption is insufficient. A $CsPbBr_3$ film that is too thin yields fewer electrons and holes due to insufficient sunlight absorption, resulting in a low current density.[24] The light absorption efficiency increases with the increase in thickness; as a result, J_{sc} and PCE are significantly improved.[35,36] When the thickness of the $CsPbBr_3$ layer exceeds 200 nm, the predominant reason for the reduction of the efficiency of the thicker device is that the absorption depth of $CsPbBr_3$ mismatches the diffusion length of the carrier.[37,38] The diffusion length of $CsPbBr_3$ is reported to be ~200 nm.[39] When the thickness is appropriate, the TiO_2 electron transport layer absorbs most of the electrons before they combine.[33] However, when the thickness of the $CsPbBr_3$ layer is larger than 200 nm, exceeding the diffusion length, the carriers (electrons and holes) generated inside the $CsPbBr_3$ layer combine again before they reach the electrode and cannot be efficiently collected by the ETL and HTL. Thus, a sharp decrease of PCE and J_{sc} with increasing thickness is observed. From the above results, it can be seen that 200 nm is the optimum thickness of the $CsPbBr_3$ layer. Figure 7a,b shows that the $J-V$ curve and IPCE spectrum of the best devices with the optimum thickness of m-TiO_2 layer and perovskite layer, with J_{sc} of 6.4 mA cm^{-2}, V_{oc} of 1.37 V, FF of 72%, and PCE of 6.3%, have been obtained.

4. CONCLUSION

In summary, PLD has been successfully applied to prepare the $CsPbBr_3$ layer instead of the conventional spin-coating method. The thin and dense $CsPbBr_3$ films prepared by PLD display good stability in high humidity. The structural characterizations have confirmed the preparation of a dense and uniform $CsPbBr_3$ layer, which totally penetrates into the m-TiO_2 layer with uniform distribution. By optimizing the device parameters, the highest PCE value of 6.3% with J_{sc} of 6.4 mA cm^{-2}, V_{oc} of 1.37 V, and FF of 72% under one sun illumination is achieved, when the thicknesses of the m-TiO_2 and $CsPbBr_3$ layers are both 200 nm. The successful application of PLD for preparation of the $CsPbBr_3$ layer may advance the large-area PSC fabrication. Further experiments are still undertaken to prepare all the layers, including the ETL and HTL, etc., by PLD to avoid the break of the vacuum condition during device fabrication for higher performance.

■ ASSOCIATED CONTENT

Supporting Information

The Supporting Information is available free of charge on the ACS Publications website at DOI: 10.1021/acsaem.9b00130.

Additional results including EDX data; PL; photographs; and SEM, AFM, and SEM images (PDF)

DOI: 10.1021/acsaem.9b00130
ACS Appl. Energy Mater. 2019, 2, 2305−2312

AUTHOR INFORMATION

Corresponding Authors

*E-mail: zhanghaophysics@hotmail.com (H.Z.).
*E-mail: xuqingyu@seu.edu.cn (Q.X.).

ORCID

Hong Wang: 0000-0003-0694-5227
Shuai Dong: 0000-0002-6910-6319
Hao Zhang: 0000-0003-1693-3545

Author Contributions

The manuscript was written through contributions of all authors. All authors have given approval to the final version of the manuscript.

Notes

The authors declare no competing financial interest.

ACKNOWLEDGMENTS

This work is supported by the National Natural Science Foundation of China (51771053, 51471085), the National Key Research and Development Program of China (2016YFA0300803), the Fundamental Research Funds for the Central Universities, and the open research fund of the Key Laboratory of MEMS of Ministry of Education, Southeast University.

REFERENCES

(1) Zhang, H.; Wang, H.; Ma, M.; Wu, Y.; Dong, S.; Xu, Q. Application of Compact TiO_2 Layer Fabricated by Pulsed Laser Deposition in Organometal Trihalide Perovskite Solar Cells. *Sol. RRL* **2018**, *2*, 1800097.

(2) Ma, Q.; Huang, S.; Wen, X.; Green, M. A.; Ho-Baillie, A. W. Y. Hole Transport Layer Free Inorganic $CsPbIBr_2$ Perovskite Solar Cell by Dual Source Thermal Evaporation. *Adv. Energy Mater.* **2016**, *6*, 1502202.

(3) Kirchartz, T.; Rau, U. What Makes a Good Solar Cell? *Adv. Energy Mater.* **2018**, *8*, 1703385.

(4) Chang, X.; Li, W.; Zhu, L.; Liu, H.; Geng, H.; Xiang, S.; Liu, J.; Chen, H. Carbon-Based $CsPbBr_3$ Perovskite Solar Cells: All-Ambient Processes and High Thermal Stability. *ACS Appl. Mater. Interfaces* **2016**, *8*, 33649−33655.

(5) Zhang, Z.; Chen, Z.; Zhang, J.; Chen, W.; Yang, J.; Wen, X.; Wang, B.; Kobamoto, N.; Yuan, L.; Stride, J. A.; Conibeer, G. J.; Patterson, R. J.; Huang, S. Significant Improvement in the Performance of PbSe Quantum Dot Solar Cell by Introducing a $CsPbBr_3$ Perovskite Colloidal Nanocrystal Back Layer. *Adv. Energy Mater.* **2017**, *7*, 1601773.

(6) Huang, G.; Wang, C.; Zhang, H.; Xu, S.; Xu, Q.; Cui, Y. Post-Healing of Defects: An Alternative Way for Passivation of Carbon-Based Mesoscopic Perovskite Solar Cells *via* Hydrophobic Ligand Coordination. *J. Mater. Chem. A* **2018**, *6*, 2449−2455.

(7) Ke, W.; Xiao, C.; Wang, C.; Saparov, B.; Duan, H.-S.; Zhao, D.; Xiao, Z.; Schulz, P.; Harvey, S. P.; Liao, W.; Meng, W.; Yu, Y.; Cimaroli, A. J.; Jiang, C.-S.; Zhu, K.; Al-Jassim, M.; Fang, G.; Mitzi, D. B.; Yan, Y. Employing Lead Thiocyanate Additive to Reduce the Hysteresis and Boost the Fill Factor of Planar Perovskite Solar Cells. *Adv. Mater.* **2016**, *28*, 5214−5221.

(8) Lei, J.; Gao, F.; Wang, H.; Li, J.; Jiang, J.; Wu, X.; Gao, R.; Yang, Z.; Liu, S. (Frank). Efficient Planar $CsPbBr_3$ Perovskite Solar Cells by Dual-Source Vacuum Evaporation. *Sol. Energy Mater. Sol. Cells* **2018**, *187*, 1−8.

(9) Liu, C.; Li, W.; Zhang, C.; Ma, Y.; Fan, J.; Mai, Y. All-Inorganic $CsPbI_2Br$ Perovskite Solar Cells with High Efficiency Exceeding 13%. *J. Am. Chem. Soc.* **2018**, *140*, 3825−3828.

(10) Duan, J.; Dou, D.; Zhao, Y.; Wang, Y.; Yang, X.; Yuan, H.; He, B.; Tang, Q. Spray-Assisted Deposition of $CsPbBr_3$ Films in Ambient Air for Large-Area Inorganic Perovskite Solar Cells. *Mater. Today Energy* **2018**, *10*, 146−152.

(11) Li, H.; Shi, W.; Huang, W.; Yao, E.-P.; Han, J.; Chen, Z.; Liu, S.; Shen, Y.; Wang, M.; Yang, Y. Carbon Quantum Dots/TiO_x Electron Transport Layer Boosts Efficiency of Planar Heterojunction Perovskite Solar Cells to 19%. *Nano Lett.* **2017**, *17*, 2328−2335.

(12) Hoffman, J. B.; Zaiats, G.; Wappes, I.; Kamat, P. V. $CsPbBr_3$ Solar Cells: Controlled Film Growth through Layer-by-Layer Quantum Dot Deposition. *Chem. Mater.* **2017**, *29*, 9767−9774.

(13) Chen, J.; Morrow, D. J.; Fu, Y.; Zheng, W.; Zhao, Y.; Dang, L.; Stolt, M. J.; Kohler, D. D.; Wang, X.; Czech, K. J.; Hautzinger, M. P.; Shen, S.; Guo, L.; Pan, A.; Wright, J. C.; Jin, S. Single-Crystal Thin Films of Cesium Lead Bromide Perovskite Epitaxially Grown on Metal Oxide Perovskite ($SrTiO_3$). *J. Am. Chem. Soc.* **2017**, *139*, 13525−13532.

(14) Chakrabartty, J.; Harnagea, C.; Celikin, M.; Rosei, F.; Nechache, R. Improved Photovoltaic Performance from Inorganic Perovskite Oxide Thin Films with Mixed Crystal Phases. *Nat. Photonics* **2018**, *12*, 271−276.

(15) Soe, C. M. M.; Stoumpos, C. C.; Kepenekian, M.; Traoré, B.; Tsai, H.; Nie, W.; Wang, B.; Katan, C.; Seshadri, R.; Mohite, A. D.; Even, J.; Marks, T. J.; Kanatzidis, M. G. New Type of 2D Perovskites with Alternating Cations in the Interlayer Space, $(C(NH_2)_3)(CH_3NH_3)_nPb_nI_{3n+1}$: Structure, Properties, and Photovoltaic Performance. *J. Am. Chem. Soc.* **2017**, *139*, 16297−16309.

(16) Zhang, J.; Bai, D.; Jin, Z.; Bian, H.; Wang, K.; Sun, J.; Wang, Q.; Liu, S. F. 3D-2D-0D Interface Profiling for Record Efficiency All-Inorganic $CsPbBrI_2$ Perovskite Solar Cells with Superior Stability. *Adv. Energy Mater.* **2018**, *8*, 1703246.

(17) Kulbak, M.; Cahen, D.; Hodes, G. How Important Is the Organic Part of Lead Halide Perovskite Photovoltaic Cells? Efficient $CsPbBr_3$ Cells. *J. Phys. Chem. Lett.* **2015**, *6*, 2452−2456.

(18) Chen, M.; Ju, M.-G.; Carl, A. D.; Zong, Y.; Grimm, R. L.; Gu, J.; Zeng, X. C.; Zhou, Y.; Padture, N. P. Cesium Titanium(IV) Bromide Thin Films Based Stable Lead-Free Perovskite Solar Cells. *Joule* **2018**, *2*, 558−570.

(19) Bian, H.; Bai, D.; Jin, Z.; Wang, K.; Liang, L.; Wang, H.; Zhang, J.; Wang, Q.; Liu, S. (Frank). Graded Bandgap $CsPbI^{2+}Br^{1-}$ Perovskite Solar Cells with a Stabilized Efficiency of 14.4%. *Joule* **2018**, *2*, 1500−1510.

(20) Lau, C. F. J.; Deng, X.; Ma, Q.; Zheng, J.; Yun, J. S.; Green, M. A.; Huang, S.; Ho-Baillie, A. W. Y. $CsPbIBr_2$ Perovskite Solar Cell by Spray-Assisted Deposition. *ACS Energy Lett.* **2016**, *1*, 573−577.

(21) Suda, Y.; Kawasaki, H.; Ueda, T.; Ohshima, T. Preparation of High Quality Nitrogen Doped TiO_2 Thin Film as a Photocatalyst Using a Pulsed Laser Deposition Method. *Thin Solid Films* **2004**, *453−454*, 162−166.

(22) Kitazawa, S.; Choi, Y.; Yamamoto, S. In Situ Optical Spectroscopy of PLD of Nano-Structured TiO_2. *Vacuum* **2004**, *74*, 637−642.

(23) Dirin, D. N.; Cherniukh, I.; Yakunin, S.; Shynkarenko, Y.; Kovalenko, M. V. Solution-Grown $CsPbBr_3$ Perovskite Single Crystals for Photon Detection. *Chem. Mater.* **2016**, *28*, 8470−8474.

(24) Liu, M.; Johnston, M. B.; Snaith, H. J. Efficient Planar Heterojunction Perovskite Solar Cells by Vapour Deposition. *Nature* **2013**, *501*, 395−398.

(25) Ouyang, Y.; Li, Y.; Zhu, P.; Li, Q.; Gao, Y.; Tong, J.; Shi, L.; Zhou, Q.; Ling, C.; Chen, Q.; Deng, Z.; Tan, H.; Deng, W.; Wang, J. Photo-Oxidative Degradation of Methylammonium Lead Iodide Perovskite: Mechanism and Protection. *J. Mater. Chem. A* **2019**, *7*, 2275−2282.

(26) Zhang, H.; Tao, M.; Gao, B.; Chen, W.; Li, Q.; Xu, Q.; Dong, S. Preparation of $CH_3NH_3PbI_3$ Thin Films with Tens of Micrometer Scale at High Temperature. *Sci. Rep.* **2017**, *7*, 8458.

(27) Yang, D.; Yang, R.; Zhang, J.; Yang, Z.; Liu, S.; Li, C. High Efficiency Flexible Perovskite Solar Cells Using Superior Low Temperature TiO_2. *Energy Environ. Sci.* **2015**, *8*, 3208−3214.

(28) Salado, M.; Calió, L.; Contreras-Bernal, L.; Idígoras, J.; Anta, J.; Ahmad, S.; Kazim, S. Understanding the Influence of Interface

DOI: 10.1021/acsaem.9b00130
ACS Appl. Energy Mater. 2019, 2, 2305−2312

Morphology on the Performance of Perovskite Solar Cells. *Materials* **2018**, *11*, 1073.
(29) Kim, H.-S.; Park, N.-G. Parameters Affecting $I - V$ Hysteresis of $CH_3NH_3PbI_3$ Perovskite Solar Cells: Effects of Perovskite Crystal Size and Mesoporous TiO_2 Layer. *J. Phys. Chem. Lett.* **2014**, *5*, 2927−2934.
(30) Zhang, F.; Yang, X.; Wang, H.; Cheng, M.; Zhao, J.; Sun, L. Structure Engineering of Hole−Conductor Free Perovskite-Based Solar Cells with Low-Temperature-Processed Commercial Carbon Paste As Cathode. *ACS Appl. Mater. Interfaces* **2014**, *6*, 16140−16146.
(31) Zhu, L.; Shi, J.; Li, D.; Meng, Q. Effect of Mesoporous TiO_2 Layer Thickness on the Cell Performance of Perovskite Solar Cells. *Huaxue Xuebao* **2015**, *73*, 261.
(32) Liang, J.; Wang, C.; Wang, Y.; Xu, Z.; Lu, Z.; Ma, Y.; Zhu, H.; Hu, Y.; Xiao, C.; Yi, X.; Zhu, G.; Lv, H.; Ma, L.; Chen, T.; Tie, Z.; Jin, Z.; Liu, J. All-Inorganic Perovskite Solar Cells. *J. Am. Chem. Soc.* **2016**, *138*, 15829−15832.
(33) Liu, D.; Gangishetty, M. K.; Kelly, T. L. Effect of $CH_3NH_3PbI_3$ Thickness on Device Efficiency in Planar Heterojunction Perovskite Solar Cells. *J. Mater. Chem. A* **2014**, *2*, 19873−19881.
(34) Kumar, M. H.; Yantara, N.; Dharani, S.; Graetzel, M.; Mhaisalkar, S.; Boix, P. P.; Mathews, N. Flexible, Low-Temperature, Solution Processed ZnO-Based Perovskite Solid State Solar Cells. *Chem. Commun.* **2013**, *49*, 11089.
(35) Boix, P. P.; Lee, Y. H.; Fabregat-Santiago, F.; Im, S. H.; Mora-Sero, I.; Bisquert, J.; Seok, S. I. From Flat to Nanostructured Photovoltaics: Balance between Thickness of the Absorber and Charge Screening in Sensitized Solar Cells. *ACS Nano* **2012**, *6*, 873−880.
(36) Mora-Seró, I.; Bisquert, J.; Fabregat-Santiago, F.; Garcia-Belmonte, G.; Zoppi, G.; Durose, K.; Proskuryakov, Y.; Oja, I.; Belaidi, A.; Dittrich, T.; Tena-Zaera, R.; Katty, A.; Levy-Clement, C.; Barrioz, V.; Irvine, S. J. C. Implications of the Negative Capacitance Observed at Forward Bias in Nanocomposite and Polycrystalline Solar Cells. *Nano Lett.* **2006**, *6*, 640−650.
(37) Stranks, S. D.; Eperon, G. E.; Grancini, G.; Menelaou, C.; Alcocer, M. J. P.; Leijtens, T.; Herz, L. M.; Petrozza, A.; Snaith, H. J. Electron-Hole Diffusion Lengths Exceeding 1 Micrometer in an Organometal Trihalide Perovskite Absorber. *Science* **2013**, *342*, 341−344.
(38) Xing, G.; Mathews, N.; Sun, S.; Lim, S. S.; Lam, Y. M.; Gratzel, M.; Mhaisalkar, S.; Sum, T. C. Long-Range Balanced Electron and Hole Transport Lengths in Organic-Inorganic CH3NH3PbI3. *Science* **2013**, *342*, 344−347.
(39) Li, B.; Zhang, Y.; Zhang, L.; Yin, L. $PbCl_2$ -Tuned Inorganic Cubic $CsPbBr_3$ (Cl) Perovskite Solar Cells with Enhanced Electron Lifetime, Diffusion Length and Photovoltaic Performance. *J. Power Sources* **2017**, *360*, 11−20.

DOI: 10.1021/acsaem.9b00130
ACS Appl. Energy Mater. 2019, 2, 2305−2312